Available online at www.sciencedirect.com
SCIENCE DIRECT
Journal of the European Ceramic Society 26 (2006) 1069–1074
www.elsevier.com/locate/jeurceramsoc

# Effect of chemical composition of intergranular glass on superplastic compressive deformation of β-silicon nitride

E. Narimatsu*, Y. Shinoda, T. Akatsu, F. Wakai

*Center for Materials Design, Materials and Structures Laboratory, Tokyo Institute of Technology, R3-23, 4259 Nagatsuta, Midori, Yokohama 226-8503, Japan*

Received 27 July 2004; received in revised form 5 November 2004; accepted 21 November 2004
Available online 21 January 2005

**Abstract**

The effect of chemical composition of $Y_2O_3$–$Al_2O_3$–$SiO_2$-based intergranular glass on superplastic deformation of β-$Si_3N_4$ was studied by compression tests at 1873 K. All hot isostatically pressed $Si_3N_4$ materials had essentially the same microstructure and the same amount of glass phase, which was different in composition only. The relation between flow stress and glass composition qualitatively corresponded to the effect of chemical composition on viscosity of $Y_2O_3$–$Al_2O_3$–$SiO_2$ glass. However, the flow stress was not proportional to the viscosity of $Y_2O_3$–$Al_2O_3$–$SiO_2$ glass, probably because the composition of intergranular glass phase had changed by dissolving $Si_3N_4$. The strain hardening (increase of flow stress with deformation) was dependent on the chemical composition of intergranular glass. Actually, the apparent strain hardening was not proportional to the strain but was proportional to time. The crystallization of $Si_2N_2O$ was also proportional to time, and was dependent on the chemical composition of the intergranular glass in a similar way to the strain hardening. Thus, it was suggested that the crystallization of $Si_2N_2O$ reduced the amount of the intergranular glass, thereby increasing flow stress.


*Keywords:* Superplasticity; $Si_3N_4$; Glass

## 1. Introduction

Silicon nitride ($Si_3N_4$) is usually sintered with the aid of oxide additives, which provide a liquid phase during sintering and promote the densification. The glass phase often remains in the microstructure after sintering, and affects the physical properties of $Si_3N_4$. Strength and creep resistance at elevated temperatures can be improved by optimizing glass composition, it's amount, and heat treatments.[1] On the other hand, the superplastic $Si_3N_4$ have been developed by using $Y_2O_3$–$Al_2O_3$,[2–7] $Y_2O_3$–MgO,[8,9] MgO–$Al_2O_3$–$SiO_2$,[10] $Y_2O_3$–$MgAl_2O_4$,[11] $Y_2O_3$–$Al_2O_3$–AlN,[12] $Y_2O_3$–$Al_2O_3$–AlN–$LiO_2$[13] as sintering additives. Superplasticity refers to the ability of some polycrystalline materials to exhibit extraordinarily large elongation. Among them, $Y_2O_3$–$Al_2O_3$ has often been chosen as sintering additives, and Y–Al–Si–O–N glass phase is formed at grain boundaries. The grain boundary glassy phase plays an important role in the superplasticity of silicon nitride. The glass phase forms a pocket at triple junctions and a glass film with the equilibrium thickness of several nm at two-grain junction.[14] The glass phase acts as a lubricant for grain boundary sliding, and also as a path for matter transport through solution-precipitation process.

The aim of this paper is to study the effect of chemical composition of intergranular glass on superplastic compressive deformation of β-$Si_3N_4$. Oxide additives were used to form $Y_2O_3$–$Al_2O_3$–$SiO_2$ melts, and, with increasing temperatures, an oxynitride melts (Y–Al–Si–O–N) by dissolving $Si_3N_4$. The relationship between the viscosity of melts and the superplastic deformation was discussed in this paper.

* Corresponding author.
*E-mail address:* nari@msl.titech.ac.jp (E. Narimatsu).

0955-2219/$ – see front matter © 2004 Elsevier Ltd. All rights reserved.
doi:10.1016/j.jeurceramsoc.2004.11.016

Table 1
Characteristics of $Y_2O_3$–$Al_2O_3$–$SiO_2$ glasses

| Material | Chemical composition (mol%) | $Y_2O_3/Al_2O_3$ mole ratio | $SiO_2/Al_2O_3$ mole ratio | Density (g/cm$^3$) | Melting temperature (K) |
|---|---|---|---|---|---|
| A | $54SiO_2{\cdot}26Al_2O_3{\cdot}20Y_2O_3$ | 0.76 | 2.07 | 3.28 | 1623 |
| B | $70SiO_2{\cdot}17Al_2O_3{\cdot}13Y_2O_3$ | 0.76 | 4.11 | 2.97 | 1723 |
| C | $89SiO_2{\cdot}8Al_2O_3{\cdot}3Y_2O_3$ | 0.37 | 11.1 | 2.43 | 1863 |

## 2. Experimental procedure

### 2.1. Materials

The fine β-$Si_3N_4$ powder was prepared by grinding submicrometer β-powder (NP-500, Denki Kagaku Kogyo Co., Tokyo, Japan) in anhydrous ethanol in a $Si_3N_4$ pot with $Si_3N_4$ balls for 20 h at a speed of 280 rpm using a planetary ball-mill. The average particle size of obtained fine β-$Si_3N_4$ was 104 nm, and the powder contained 0.88 wt.% oxygen. We assumed that this oxygen existed as $SiO_2$ on the surface of the powder. The powder was mixed with $Y_2O_3$ (RU grade, Shin-Etsu Chemical Co., Tokyo, Japan), $Al_2O_3$ (AKP-50, Sumitomo Chemical Co., Tokyo, Japan), and $SiO_2$ (Kojundo Chemical Laboratory Co., Saitama, Japan) as sintering additives, and then mixed in an anhydrous ethanol for 1 h by using a planetary ball-mill. The slurry was dried at about 343 K with hot plate, then, granulated.

The amount of additives was adjusted so that the volume fraction of grain boundary glass phase was 15 vol.%. Although $Si_3N_4$ dissolved into oxide melt, we assumed that the density of grain boundary glass phase was close to the density of the oxide glass calculated by Appen's formula.[15] Table 1 shows the compositions of three glasses (A, B, C) chosen in this study. The melting temperature of glass ($T_m$) was estimated by liquidus temperature in $Y_2O_3$–$Al_2O_3$–$SiO_2$ ternary phase diagram.[16] Fig. 1 illustrates the compositions of these three glasses in the ternary phase diagram.

The powder compacts were formed by die pressing at 30 MPa, followed by cold isostatically pressing (CIP) at 200 MPa. The green compacts were coated with BN powder, and then encapsulated by borosilicate glass at 973 K. They were hot isostatically pressed (HIPed) under Ar gas. The samples were heated up to 1073 K, then, pressure was applied to 200 MPa. The temperature for hot isostatically pressing was 1973 K, and the sample was kept for 1 h.

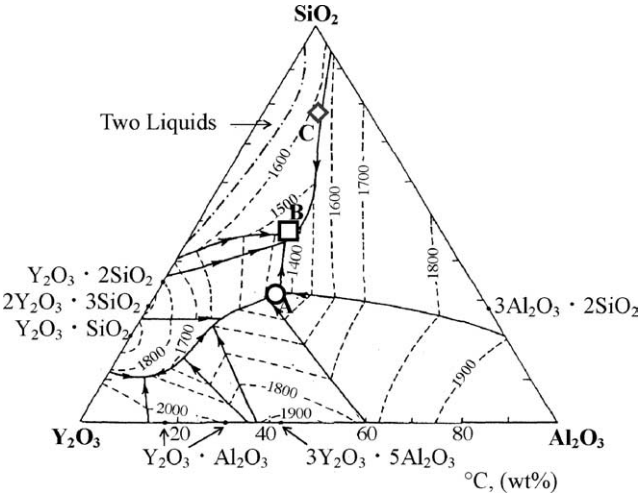


Fig. 1. Composition of $Y_2O_3$–$Al_2O_3$–$SiO_2$ glass ((◯) A, (□) B, (◊) C).

### 2.2. Mechanical testing

The sintered bodies were cut into rectangular bars with dimensions of 2 mm × 2 mm × 3 mm. The specimens were placed between two SiC platens. BN powder was deposited onto the samples before testing, in order to avoid barreling of the compressed sample. The specimens were heated up to a test temperature at a rate of 30 K/min, then, the compression tests were performed by using a universal testing machine at constant crosshead speed in $N_2$ (1 atm) at 1873 K.

### 2.3. Microstructural characterization

Phase identification of the samples before and after deformation was conducted by using X-ray diffractometry (XRD). The volume fraction of $Si_2N_2O$ was determined by XRD using calibration lines.[17,18] Scanning electron microscopy (SEM) was used for microstructural characterization of the samples before and after deformation. The polished samples were plasma-etched with $CF_4$ that contained oxygen gas. The grain size was defined as the diameter of equivalent circle. The length ($L$) and width ($W$) of each grain were measured, and the aspect ratio of grain was defined as the ratio of length to width ($L/W$). The average of 500 grains was used for calculating the average grain size and the aspect ratio.

The amounts of oxygen content in the fine β-$Si_3N_4$ powder and test samples were measured by oxygen/nitrogen determinator (TC-436 type, LECO Co.).

## 3. Results and discussion

### 3.1. Effect of viscosity of intergranular glass on flow stress

The microstructural characteristics of as-HIPed materials (A, B, C) are summarized in Table 2. All materials were fully densified by hot isostatically pressing. The microstructures of as-HIPed materials are shown in Fig. 2. Materials A, B, and C are mainly consisted of equiaxed grains, and contained some rod-shaped grains. The average grain size and the as-

Table 2
Characteristics of HIPed β-$Si_3N_4$ materials

| Material | Density (g/cm$^3$) | Grain size (nm) | Aspect ratio | Phase (vol.%) | Oxygen content (wt.%) |
|---|---|---|---|---|---|
| A | 3.17 | 205 | 1.74 | β-$Si_3N_4$ (83.6), $Si_2N_2O$ (2.1), glass (14.3) | 5.86 |
| B | 3.07 | 214 | 1.76 | β-$Si_3N_4$ (83.1), $Si_2N_2O$ (2.9), glass (14.0) | 6.27 |
| C | 3.05 | 220 | 1.96 | β-$Si_3N_4$ (82.4), $Si_2N_2O$ (3.9), glass (13.7) | 6.56 |

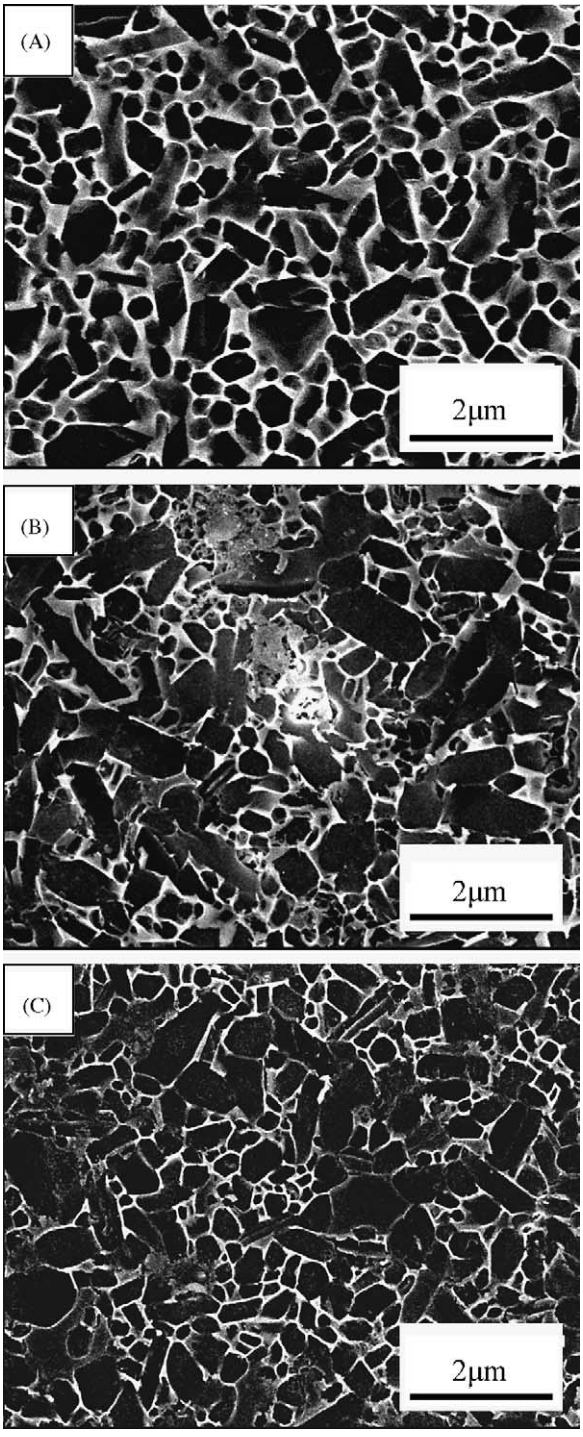


Fig. 2. SEM micrograph of as-HIPed materials. The materials (A, B, C) had essentially the same microstructure and the same amount of glass phase which was different in composition only.

pect ratio of all materials (A, B, C) were approximately the same as shown in Table 2. All materials contained mostly β-$Si_3N_4$, and small amount of $Si_2N_2O$. No α-$Si_3N_4$ was detected. The three materials (A, B, C) had essentially the same microstructure and the same amount of glass phase which was different in composition only.

The compression tests were performed at 1873 K, which was higher than the melting temperature of $Y_2O_3$–$Al_2O_3$–$SiO_2$ glasses. A typical set of true stress–true strain curves at 1873 K is shown in Fig. 3. Strain hardening, which is the increase of stress with deformation, was observed during the deformation of all three materials. The strain hardening suggests that the microstructural evolution occurs during the deformation. However, we can assume that the initial microstructure is maintained at the very beginning of deformation. Since the materials (A, B, C) had essentially the same microstructure, the difference in the initial flow stress $\sigma_0$ (flow stress at true strain is equal to 0.03) could be due to the difference in composition of intergranular glass. In the high-temperature deformation of silicon nitride, it has been believed that the flow stress $\sigma_0$ is proportional to the viscosity $\eta$ of intergranular glass,[19,20]

$$\sigma_0 = A\dot{\varepsilon}_0 \eta d^P, \quad (1)$$

where $\dot{\varepsilon}_0$ the initial strain rate, $d$ the grain size, $p$ the exponent of the grain size, and $A$ is a constant. We examined the relation between the flow stress and the viscosity of $Y_2O_3$–$Al_2O_3$–$SiO_2$ melt. Saito et al.[21] reported the influence of the chemical composition on the viscosity of $Y_2O_3$–$Al_2O_3$–$SiO_2$ melts and Y–Al–Si–O–N melts recently. Saito's results on viscosity was plotted as a function of $Y_2O_3/Al_2O_3$ mole ratio in Fig. 4. The viscosity decreased with increasing $Y_2O_3/Al_2O_3$ mole ratio, when $SiO_2/Al_2O_3$ mole ratio was fixed. The glass phase in materials A and B had $Y_2O_3/Al_2O_3$ mole ratio of 0.76, and that in mate-

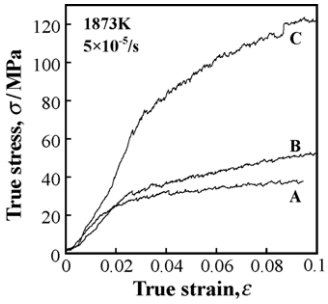


Fig. 3. True stress–true strain curves of materials A, B, and C at 1873 K and at $5 \times 10^{-5}$/s.

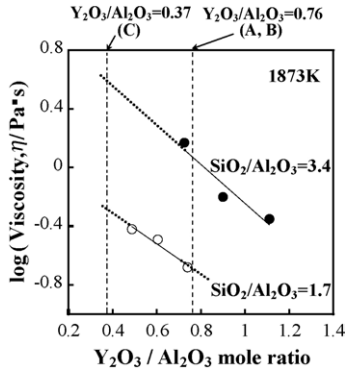


Fig. 4. Viscosity of $Y_2O_3$–$Al_2O_3$–$SiO_2$ glass ((◯) $SiO_2/Al_2O_3 = 1.7$, (●) $SiO_2/Al_2O_3 = 3.4$) as a function of $Y_2O_3/Al_2O_3$ mole ratio. Dashed line represents $Y_2O_3/Al_2O_3$ mole ratio of A and B and alternate long and short dash line represents $Y_2O_3/Al_2O_3$ mole ratio of C.

rial C had $Y_2O_3/Al_2O_3$ mole ratio of 0.37. The viscosities at $Y_2O_3/Al_2O_3$ mole ratio is equal to 0.76 and 0.37 were read from Fig. 4, and were plotted as open triangles and open squares in Fig. 5, respectively. The viscosity of $Y_2O_3$–$Al_2O_3$–$SiO_2$ melt increased with the increase in $SiO_2/Al_2O_3$ mole ratio, when $Y_2O_3/Al_2O_3$ mole ratio was fixed. Initial flow stress was also plotted in Fig. 5. When the materials A and B, which have the same $Y_2O_3/Al_2O_3$ mole ratio is equal to 0.76, are compared, material A with lower $SiO_2/Al_2O_3$ mole ratio deformed at lower stress than that of material B with higher $SiO_2/Al_2O_3$ mole ratio. The flow stress of material C was much higher than that of materials A and B, because the glass phase in material C had higher $SiO_2/Al_2O_3$ mole ratio and lower $Y_2O_3/Al_2O_3$ mole ratio. Although flow stress also increased with increasing $SiO_2/Al_2O_3$ mole ratio, the rate of increase of flow stress was much lower than the rate of increase of viscosity of $Y_2O_3$–$Al_2O_3$–$SiO_2$ melt. Since the chemical composition of glass phase can be altered during sintering, the flow stress may not be proportional to the viscosity of initial $Y_2O_3$–$Al_2O_3$–$SiO_2$ melt. $Si_3N_4$ dissolves into grain boundary glass phase, then, the glass phase contains nitrogen.

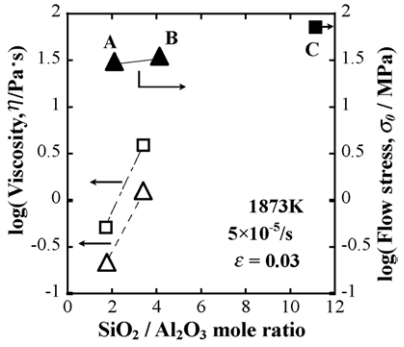


Fig. 5. Flow stress (▲) A,B($Y_2O_3/Al_2O_3 = 0.76$), (■) C($Y_2O_3/Al_2O_3 = 0.37$) and viscosity of $Y_2O_3$–$Al_2O_3$–$SiO_2$ glass (△) ($Y_2O_3/Al_2O_3 = 0.76$), (□) ($Y_2O_3/Al_2O_3 = 0.37$) as a function of $SiO_2/Al_2O_3$ mole ratio.

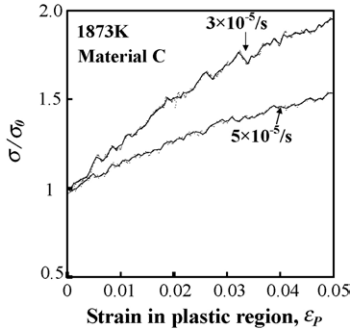


Fig. 6. Flow stress normalized by the initial stress $\sigma_0$ as a function of strain in plastic deformation region at 1873 K for material C. The apparent "strain hardening" was dependent on strain rate.

Saito and co-workers reported that the solubility of nitrogen into $Y_2O_3$–$Al_2O_3$–$SiO_2$ melts was 7–9 mol%. The viscosity of Y–Al–Si–O–N melt increased in proportion to a nitrogen content. The saturated nitrogen content depends on glass composition. The saturated nitrogen increased with the decreasing $SiO_2/Al_2O_3$ mole ratio at a constant $Y_2O_3$ content. We suppose that the viscosity of Y–Al–Si–O–N melt in material A, which has lower $SiO_2/Al_2O_3$ mole ratio, has been increased more significantly than that in material B. Therefore, the difference between flow stresses of materials A and B with Y–Al–Si–O–N melt was smaller than the difference between viscosities of $Y_2O_3$–$Al_2O_3$–$SiO_2$ melt in materials A and B.

### 3.2. Apparent strain hardening by crystallization

Strain hardening was observed in the true stress–true strain curves in Fig. 3. Strain hardening was the most significant in material C, while material A deformed at almost constant stress. Fig. 6 shows the normalized stress $\sigma/\sigma_0$ versus plastic strain $\varepsilon_P$ curves for material C at different strain rates, where $\sigma_0$ is the initial stress at $\varepsilon = 0.03$ in Fig. 3, and $\varepsilon_P = \varepsilon - 0.03$. The apparent strain hardening, or the slope of curve, was dependent on strain rate, and increased with decreasing strain rate. Fig. 7 shows the increase of normalized stress $\sigma/\sigma_0$ with time at different strain rates for material C. The apparent "strain hardening" was proportional to time. The slope of curves was approximately the same independent of strain rate. The increase of stress was proportional to time and independent of strain rate also in materials A and B.

Fig. 8 shows the increase of $Si_2N_2O$ after deformation with time. The initial $Si_2N_2O$ contents were A (2.1 vol.%), B (2.9 vol.%), and C (3.9 vol.%), respectively. The increase of $Si_2N_2O$ content was the smallest in material A, and was the largest in material C. The material B was intermediate between materials A and C. There was a good correlation between strain hardening and crystallization of $Si_2N_2O$, because the strain hardening was smallest in material A and was the largest in material C as shown in Fig. 3. Furthermore, the volume fraction of $Si_2N_2O$ increases with time after nucleation.[17] Since, both crystallization and apparent

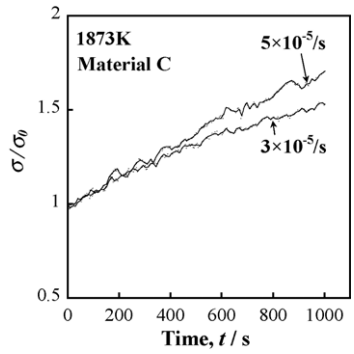


Fig. 7. Flow stress of material C normalized by the initial stress $\sigma_0$ as a function of testing time in plastic deformation region at 1873 K.

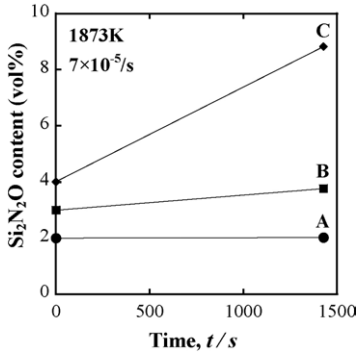


Fig. 8. $Si_2N_2O$ content after deformation as a function of time at 1873 K.

"strain hardening" are dependent on time, we suppose that the increase of flow stress with time is related to crystallization of $Si_2N_2O$.

Here, we consider the effect of crystallization of $Si_2N_2O$ on deformation. Creep of silicon nitride-based ceramics has been extensively studied,[1] and it was known that creep resistance of $Y_2O_3/Al_2O_3$-fluxed $Si_3N_4$ increased remarkably by crystallization of intergranular glass phase.[22] The crystallization reduces the volume fraction of intergranular glass phase, which acts as a lubricant for grain boundary sliding, and also acts as a path for matter transport through solution-precipitation process. Thus, the deformation is impeded consequently. Since, crystallization of $Si_2N_2O$ occurred during deformation in our study, intergranular glass phase decreased with crystallization of $Si_2N_2O$ by the following reaction:

$$Si_3N_4 + SiO_2 \rightarrow 2Si_2N_2O \quad (2)$$

The decrease of intergranular glass phase by crystallization is probably the origin of strain hardening. Similar strain hardening during superplastic deformation has been observed in deformation of $Si_3N_4$–$SiO_2$–$MgAl_2O_4$ (1.0:1.0:0.1–0.3 mol%) material also.[18] On the other hand, Xie and co-workers reported that strain hardening did not take place in spite of growth of elongated $Si_2N_2O$ grains. A transient Mg–Al–Si–O–N liquid phase was present during deformation. They concluded that the transient liquid greatly enhanced the high-temperature viscoplastic flow and reduced the flow resistance. However, in our study, the chemical composition of liquid phase (Y–Al–Si–O–N) differs from Xie's material. Probably, the difference in chemical composition of the intergranular liquid phase is responsible to the difference in effect of crystallization on deformation.

Here, we discuss the effect of grain growth on strain hardening. The average grain size and the aspect ratio of grains remained nearly constant after deformation as shown in Fig. 9. We also measured the average grain size and the aspect ratio for 10% of largest grains, and found that both parameters also remained constant after deformation. These results showed that the strain hardening did not occur due to grain growth.

The oxygen content decreased during deformation as shown in Fig. 10. Oxygen loss was defined as the ratio of the decrease of oxygen content after deformation to the initial oxygen content of the sample. The initial oxygen content was summarized in Table 2. The oxygen loss suggested that the intergranular glass evaporated during deformation at 1873 K. The evaporation of intergranular glass has been usually attributed to SiO volatilization from Y–Al–Si–O–N liquid.[23] The oxygen loss was largest in material A that had the eutectic composition. The intergranular glass is a continuous path for fast diffusion of gaseous molecules. The low viscosity of glass with the eutectic composition enhances the evaporation. The SEM observation of deformed samples, especially material A, showed that pores were generated near surface. The

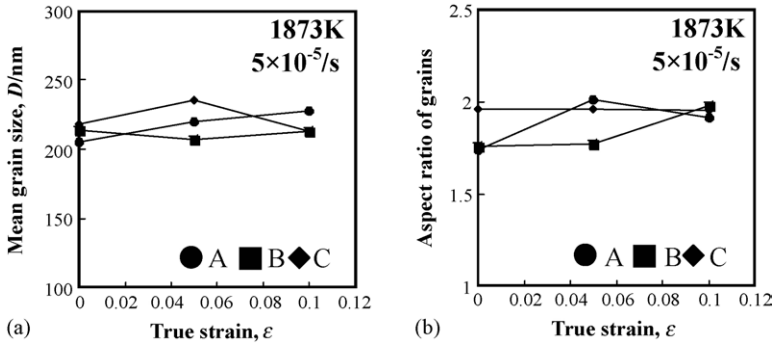


Fig. 9. (a) Mean grain size and (b) aspect ratio of grains as a function of true strain at 1873 K. The average grain size and the aspect ratio of grains remained nearly constant during deformation.

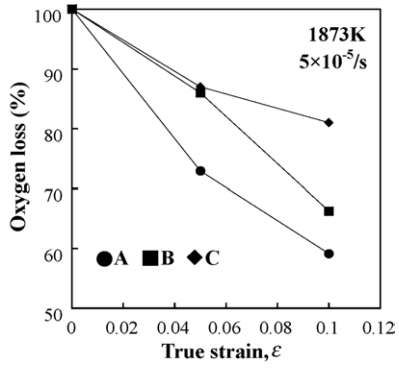


Fig. 10. Oxygen loss as a function of true strain at 1873 K.

formation of pores was the result of SiO volatilization. Since the formation of pore decreases the actual cross-sectional area of the specimen, which support stress, the flow stress decreases with increasing pore volume. Therefore, the formation of pores could not be the origin of strain hardening. The crystallization of $Si_2N_2O$, which was the origin of strain hardening, affected oxygen loss also. In material C, the evaporation of intergranular glass phase was suppressed, because the intergranular glass phase crystallized to $Si_2N_2O$. On the other hand, the evaporation of grain boundary glass phase was not suppressed in material A, which showed little crystallization.

## 4. Conclusion

The effect of chemical composition of $Y_2O_3$–$Al_2O_3$–$SiO_2$-based intergranular glass on superplastic deformation of β-$Si_3N_4$ was studied by compression tests at 1873 K. All HIPed materials had essentially the same microstructure and the same amount of glass phase, which was different in composition only. When $Y_2O_3/Al_2O_3$ mole ratio was constant, the flow stress increased with increasing $SiO_2/Al_2O_3$ mole ratio. On the other hand, the flow stress increased with decreasing $Y_2O_3/Al_2O_3$ mole ratio. The relation between flow stress and glass composition qualitatively corresponded to the effect of chemical composition on viscosity of $Y_2O_3$–$Al_2O_3$–$SiO_2$ glass. However, the rate of increase of the flow stress was not proportional to the viscosity of $Y_2O_3$–$Al_2O_3$–$SiO_2$ glass, probably because the composition of intergranular glass phase had changed by dissolving $Si_3N_4$. It was suggested that the flow stress was dependent on the viscosity of Y–Al–Si–O–N melts. We have found that apparent "strain hardening" (the increase of stress with deformation) was not proportional to the strain but was proportional to time. The crystallization of $Si_2N_2O$ was the origin of the apparent "strain hardening". The crystallization reduced the volume fraction of intergranular glass phase, which acted as a lubricant for grain boundary sliding and also as a path for matter transport through solution-precipitation process. Therefore, the crystallization increased the flow stress. The evaporation of intergranular glass phase (SiO volatilization) was suppressed by crystallization of $Si_2N_2O$.

## References

1. Meléndez-Martínez, J. J. and Domínguez-Rodríguez, A., Creep of silicon nitride. *Prog. Mater. Sci.*, 2004, **49**, 19–107.
2. Wakai, F., Komada, Y., Sakaguchi, S., Murayama, N. and Niihara, K., A superplastic covalent crystal composite. *Nature*, 1990, **344**, 421–423.
3. Rouxel, T., Wakai, F. and Izaki, K., Tensile ductility of superplastic $Al_2O_3$–$Y_2O_3$–$Si_3N_4$/SiC nanocomposite. *J. Am. Ceram. Soc.*, 1992, **75**, 2363–2372.
4. Kondo, N., Ohji, T. and Wakai, F., Deformation conditions of β-SiAlON to achieve large superplastic elongation. *J. Ceram. Soc. Jpn.*, 1998, **106**, 1040–1042.
5. Burger, P., Duclos, R. and Crampon, J., Microstructure characterization in superplastically deformed silicon nitride. *J. Am. Ceram. Soc.*, 1997, **80**, 879–885.
6. Rouxel, T., Rossignol, F., Besson, J. L. and Goursat, P., Superplastic forming of an α-phase rich silicon nitride. *J. Mater. Res.*, 1997, **12**, 480–492.
7. Kondo, N., Wakai, F., Nishioka, T. and Yamakawa, A., Superplastic $Si_3N_4$ ceramics consisting of rod-shaped grains. *J. Mater. Sci. Lett.*, 1995, **14**, 1369–1371.
8. Mitomo, M., Hirotsuru, H., Suematsu, H. and Nishimura, T., Fine-grained silicon nitride ceramics prepared from β-powder. *J. Am. Ceram. Soc.*, 1995, **78**, 211–214.
9. Zhan, G. D., Mitomo, M., Xie, R. J. and Kurashima, K., The deformation mechanisms of superplastic flow in fine-grained beta-silicon nitride ceramics. *Acta Mater.*, 2000, **48**, 2373–2382.
10. Xie, R. J., Mitomo, M. and Zhan, G. D., Superplastic deformation in silicon nitride-silicon oxynitride in situ composites. *J. Am. Ceram. Soc.*, 2000, **83**, 2529–2535.
11. Schneider, J. A. and Mukherjee, A. K., Microstructural evaluation of deformation mechanisms in silicon nitride ceramics. *Ceram. Eng. Sci. Proc.*, 1996, **17**, 341–349.
12. Chen, I. W. and Hwang, S. L., Shear thickening creep in superplastic silicon nitride. *J. Am. Ceram. Soc.*, 1992, **75**, 1073–1079.
13. Rosenflanz, A. and Chen, I. W., "Classical" superplasticity of SiAlON ceramics. *J. Am. Ceram. Soc.*, 1997, **80**, 1341–1352.
14. Clarke, D. R., On the equilibrium thickness of intergranular glass phases in ceramic materials. *J. Am. Ceram. Soc.*, 1987, **70**, 15–22.
15. Appen, A. A., *Chemistry of Glass*. Chemical Publisher, Leningrad, U.S.S.R., 1970, pp. 310.
16. *Phase Diagram for Ceramists*, *Vol. II*. The American Ceramic Society, Columbus, OH, 1969, pp. 165.
17. Emoto, H., Mitomo, M., Wang, C. M., Hirotsuru, H. and Inaba, T., Fabrication of silicon nitride-silicon oxynitride in-situ composites. *J. Eur. Ceram. Soc.*, 1998, **18**, 527–533.
18. Ohashi, M. and Iida, Y., Nucleation control for hot-working of silicon oxynitride based ceramics. *J. Mater. Res.*, 1999, **14**, 170–177.
19. Dryden, J. R., Kucerovsky, D., Wilkinson, D. S. and Watt, D. F., Creep deformation due to a viscous grain boundary phase. *Acta Metall.*, 1989, **37**, 2007–2015.
20. Raj, R. and Chyung, C. K., Solution-precipitation creep in glass ceramics. *Acta Metall.*, 1981, **29**, 159–166.
21. Saito, N., Kai, K., Furusho, S., Nakashima, K., Mori, K. and Shimizu, F., Properties of nitrogen-containing yttria–alumina–silica melts and glasses. *J. Am. Ceram. Soc.*, 2003, **86**, 711–716.
22. Rae, A. W. J. M., Thompson, D. P., Pipkin, H. J. and Jack, K. H., *Special Ceramics*, *Vol. 6*, ed. P. Popper. British Ceramic Research Association, Stoke-on-Trent, England, 1975, p. 283.
23. Yokoyama, K. and Wada, S., Solid-gas reaction during sintering of $Si_3N_4$ ceramics. Part 1. Stability of $SiO_2$, $Y_2O_3$ and $Al_2O_3$ at high temperature. *J. Ceram. Soc. Jpn.*, 2000, **108**, 6–9.